



HAL
open science

Dual low pressure plasma process for SiCN:H thin films deposition: A comparative study

Robert Hugon, Ziad Al Hallak, A. Ahmad, A. Naja, Thierry Belmonte,
Mohammed Belmahi

► To cite this version:

Robert Hugon, Ziad Al Hallak, A. Ahmad, A. Naja, Thierry Belmonte, et al.. Dual low pressure plasma process for SiCN:H thin films deposition: A comparative study. *Vacuum*, 2024, 219 (112684), pp.112684. 10.1016/j.vacuum.2023.112684 . hal-04265126

HAL Id: hal-04265126

<https://hal.univ-lorraine.fr/hal-04265126>

Submitted on 30 Oct 2023

HAL is a multi-disciplinary open access archive for the deposit and dissemination of scientific research documents, whether they are published or not. The documents may come from teaching and research institutions in France or abroad, or from public or private research centers.

L'archive ouverte pluridisciplinaire **HAL**, est destinée au dépôt et à la diffusion de documents scientifiques de niveau recherche, publiés ou non, émanant des établissements d'enseignement et de recherche français ou étrangers, des laboratoires publics ou privés.



Distributed under a Creative Commons Attribution - NonCommercial - NoDerivatives 4.0 International License

Dual low pressure plasma process for SiCN:H thin films deposition: a comparative study

Authors:

R. Hugon¹, Z. Al Hallak^{1,2}, A. Ahmad², A. Naja², T. Belmonte¹, M. Belmahi^{1*}

Affiliation:

¹ Université de Lorraine, CNRS UMR 7198, Institut Jean Lamour (IJL), Department of Chemistry and Physics of Solids and Surfaces, Plasmas-Processes-Surfaces group,

2 allée André Guinier, Campus Artem, BP 50840, 54011 Nancy Cedex, France

² Laboratoire de Physique et Modélisation, Université Libanaise, Campus Rafic Hariri - Hadath - Tripoli, Lebanon

* Corresponding author email : mohammed.belmahi@univ-lorraine.fr

« This research was funded in part, by l'Agence Nationale de la Recherche (ANR), project ANR- HD-Plasm-A-SiNOC:H. For the purpose of open access, the author has applied a CC-BY public copyright licence to any Author Accepted Manuscript (AAM) version arising from this submission.»

Abstract

SiCN:H thin films have large possibilities of applications due to their versatile chemical and physical properties. Plasma Assisted Chemical Vapor Deposition (PACVD) process widely used for SiCN:H deposition. Here we discuss on the potentialities of dual Electron Cyclotron Resonance (ECR) and Radio Frequency Magnetron Sputtering (rf MS) plasmas coupling for SiCN:H deposition in Ar/N₂/Si(CH₃)₄ gas mixture. The study is carried out by varying the autopolarisation voltage V_{bias} of the silicon target.

ECR plasma gives low deposition growth rate about 50 nm/h. The films are transparent. SiCN nanopillars with high aspect ratio are obtained.

Rf MS plasma gives high deposition growth rate up to 2200 nm/h. The films are opaque in the near UV and transparent in the visible depending on their thickness. The optical index at 630 nm is 1.95, the Tauc's band gap is 3.0 eV and do not change with V_{bias} .

Dual ECR/rf MS plasma gives high deposition growth rate up to 2300 nm/h. The films are transparent. The optical index varies between 1.7 and 2.05 at 630 nm and the Tauc's band gap decreases linearly between 4.75 and 3.4 eV with V_{bias} .

Dual ECR/rf MS plasma coupling is a very promising PACVD process for thin films deposition.

Keywords:

PACVD, plasma coupling, SiCN:H thin films, Optical Emission Spectroscopy, *in-situ* Reflectometry, FTIR, optical parameters, High resolution Transmission Electron microscopy.

Highlights

- ECR plasma permit to obtain amorphous SiCN:H nano pillars suitable for catalysis or other applications.
- High growth rate of 2 200 nm/h is obtained in RF magnetron plasma deposition. Low change is observed in optical parameters with V_{bias} .
- High deposition growth rate of 2 300 nm/h is obtained with dual ECR/Magnetron plasma. The films exhibit good transparency in the visible. A linear modulation of the optical parameters vs V_{bias} is obtained.

1 Introduction

SiCN:H thin films provide a wide range of applications due to their variable chemical composition. The properties of such films are directly connected to the ternary nature of the deposited materials. The literature is rich from papers dealing with the synthesis of such films since the first theoretical work of Liu and Cohen predicting that C_3N_4 material could be as hard as diamond [1]. However, it's very difficult to obtain with Plasma Assisted Chemical Vapor Deposition (PACVD) processes crystalline thick C_3N_4 films. The adjunction of bare silicon exposed to the $CH_4/N_2/Ar$ plasma permits to obtain the first SiCN:H thin films [2-3]. Our group have also contributed to the study on the role of silicon in CN_x and SiCN thin films synthesis [4].

In the following, we discuss about the large possibilities of applications of SiCN:H thin films in different domains due to the combination of remarkable properties:

- By varying the chemical composition, it's possible to tune the hardness of the thin films and the point of this property is still studied [5-6]. Thereby, a hardness of about 40 GPa and an elastic modulus of about 300 GPa was reported [7-8] depending on the silicon precursor and its concentration, carbon radicals and nitrogen content in the gas phase and the temperature of growth. This materials also can exhibit low friction coefficient [9-10].
- SiCN:H thin films can also have wide optical band gap varying from a low value of about 3 eV to 5 eV, from SiC:H materials to SiN:H like materials. The optical index in the visible range making them very attractive for optoelectronic applications, antireflective coatings or passivating coatings for solar photovoltaics [11-15].
- SiC:H associated with metallic elements like tungsten in a composite like structure can also be highly suited for concentrated solar power as solar absorbers, depending on their

good thermal stability, oxidation resistance at high operating temperature combined with suitable optical and mechanical properties [16-17].

- Another attractive application of these materials due to their low k properties is now in microelectronics industrial manufacturing for very large scale integrated interconnects [18-19], where very thin SiCN:H films appears more adapted to the control of porosity than the used SiN:H thin films. In all cases, the application is strongly correlated with the chemical composition, synthesis process, mechanical and optical parameters.

Our study is devoted to the synthesis of SiCN:H films for the passivation or anti reflective coatings in photovoltaics based silicon but not limited to these applications.

SiCN:H thin films are mainly synthesized by chemical vapor deposition (CVD) or reactive Physical Vapor Deposition (PVD) depending on the investigated application.

Many PACVD processes use silane as silicon gas precursor [6, 11]. However this gas is pyrophoric and needs security equipment. In many cases it is substituted by organosilicon precursors. Many review papers give an up to date view on the literature on this field and the potentialities of the CVD or MPACVD processes with organosilicon precursors in SiNOC:H thin films synthesis.[7-8]. A huge activity is done in silicon precursors synthesis adapted to the SiCN:H thin films growth without the adjunction of another gas containing elements source [20-21].

Many works have been done on SiCN thin films synthesis with radiofrequency magnetron (rfMS) plasma. Most of them are done with a silicon or silicon carbide target in Ar/N₂ gas mixture. This very useful process permits to obtain very hard materials [22-26]. The growth rate can be more than 1 μ m/h. However, the films are not transparent in the near UV range except if hydrogen is added to the gas mixture. This can be achieved in CH₄/N₂/Ar gas mixture with a silicon target.

Recently, plasma assisted atomic layer deposition (PALD) was also used for the synthesis of such films. The low growth rate obtained with this process permits to control layer by layer the deposited film permitting a better control of the thin film atomic surface termination inducing the desired physical properties for the surface functionalization [27-28].

In order to obtain the suited structure of the deposited film, the choice of the plasma process is fundamental. Then it is necessary to control the growth temperature, the flow of the organosilicon precursor, and many other operating parameters such as gas pressure, substrate voltage...

The role of deposition temperature is crucial in the obtained structure. For a temperature less than 400 C, suitable for many industrial applications, the films are amorphous. They became crystalline at higher temperature ($>800^{\circ}\text{C}$), that are often obtained after annealing the samples. In a previous work, we have deposited crystalline SiC-2H nanoparticles embedded in SiCN:H obtained in $\text{Si}(\text{CH}_3)\text{-NH-Si}(\text{CH}_3)$ and Ar gas mixture in a resonant microwave cavity plasma [29]. When low nitrogen content is introduced into the plasma, the SiC nanoparticles disappear.

To prevent from dust formation in the low pressure organosilicon plasma, that induce a polymeric phase formation, we have to limit the flow of the organosilicon. Thus the ratio between silicon and nitrogen or silicon and carbon take low value. The modulation of the gas composition permitting to obtain films with different chemical composition leading to different physical parameters is thus limited, in particular in low pressure plasma processes.

For an industrial PACVD process for SiCN:H thin film synthesis, it is necessary to have a plasma in a large volume, with low ionic bombardment, preventing the damage to the thin film during the growth, a good growth rate limiting the deposition time, and a good homogeneity on a large scale surface.

In the present work, we have developed a new PACVD process for SiCN:H thin film deposition based on dual plasma sources combining multi ECR plasma sources, and a rf MS plasma with silicon target in Ar/N₂/Si(CH₃)₄ gas mixture. The study is first conducted in ECR plasma to fix the gas composition ratio, then in the rf MS plasma to evaluate its potentialities when adding atomic silicon to the gas mixture, and finally in dual ECR/rf MS plasma. The aim of this work is to evaluate the potentialities of this new dual PACVD deposition process.

2 Material and methods

The plasma reactor used for SiCN:H thin films deposition is described in Figure 1. All the flanges are equipped with Cu seals except the top, entrance of the samples flange and bottom one which are equipped with Viton® O-ring seals. The vacuum in the chamber is obtained by means of a primary rotary pump (pumping speed 10 m³/h) and a turbomolecular one (pumping speed 230 l/s). The residual pressure is approximately 10⁻⁴ Pa. The plasma chamber volume is about 50 l. The time of reaching the limit pressure is about 0.5 h and. If it's not the case, the experiment is stopped, and the cause of the leak is investigated and eliminated.

The working pressure is fixed at a compromise value of 1.3 Pa permitting the coupling of the ECR mode and the rf MS plasma.

A two inches magnetron cathode with Si(100) target is placed horizontally and is powered by a RF generator (peak power 1 kW) working at 13.56 MHz. Four Electron Cyclotron Resonance (ECR) applicators working at the frequency of 2.45 GHz (peak power at 240 W) are distributed in the same horizontal plane at 90° from each other. The total incident power is 4x200 W. All of them are connected to a microwave divider, himself powered by a 2 KW microwave generator. The sample holder is placed 10 cm under the magnetron target. The four ECR applicators are located at halfway at 5cm from the magnetron target. The deposition temperature is fixed at 400°C by regulating the current in the ohmic heater of the substrate holder which is grounded.

The gas mixture is composed from tetramethylsilane (TMS) chemical formula Si(CH₃)₄ (purity: electronic grade), Argon (purity: 99.9999%), nitrogen (purity: 99.9999%). The total gas flow is maintained constant at 40 sccm.

We use both Si(100) (500 μm thick both sides polished) and fused silica Suprasil® substrates (1 mm thick). They are ultrasonically cleaned in acetone and ethanol during 15 min each prior to the introduction into the plasma chamber. For all the samples, the films during 1 Scanning

Electron Microscopy (SEM) measurements are carried out with a Zeiss Gemini microscope with a field effect gun, working at an accelerating voltage between 1 KV and 2 KV. Cross view and top view of the samples are obtained. The thickness of the deposited samples is evaluated from the cross view photographs.

High resolution transmission electron microscopy (HRTEM) investigations were carried out using a JEM - ARM 200F Cold FEG TEM/STEM operating at 200 kV and equipped with a spherical aberration (Cs) probe and image correctors (point resolution 0.12 nm in TEM mode and 0.078 nm in STEM mode). Energy-dispersive x-ray spectrometry (EDS) is done in this equipment giving the 2D cartography of the elements present at the films surface except hydrogen. For this analysis, cross-section TEM samples of films were prepared using a focused ion beam (FIB)- SEM dual beam system (FEI Helios 600). Only one representative sample corresponding to each process is selected for this characterisation. Due to this equipment availability, the analysis was done 6 months after thin films deposition.

Optical emission spectroscopy (OES) measurements are performed by targeting the plasma between the magnetron cathode and the sample holder with an optical fiber through a quartz window by using an Andor Mechelle 5000 spectrometer with an iStar iCCD camera. The observed OES characteristic lines of the different emitting species are summarized in Table 1.

The Fourier transform infra-red spectroscopy (FTIR) measurements are performed in the transmission mode using a Thermo Scientific Nicolet iS50 spectrometer with an internal DTGS detector. FTIR Spectra are obtained with 32 accumulations with a resolution of 4 cm^{-1} between 400 cm^{-1} and 4000 cm^{-1} wavenumber. An absorption spectra of a silicon substrate was performed before each sample analysis. We assume that the difference between the sample and the substrate spectra corresponds to the vibration modes of the SiCN:H film components.

The spectrum deconvolution of the large band located between 400 and 1300 cm^{-1} called the fingerprint was carried out assuming a sum of different Gaussian lines corresponding to the

different vibration modes detected in this region. In table 2, one can find the considered bonds we have used in this study according to the work of Coustel *et al* [30] and ref. there in which synthesize many works done in this field. The deconvolution was carried out thanks to Mathlab® facilities. We have limited the FWHM to reasonable value according to table 2.

During the growth, the reflectance of the silicon substrate/SiCN:H system is followed *in-situ* by reflectometry measurements at an incidence angle of 45°. A DH-2000-BAL (Ocean Optics) white source covering the 200-1000 nm with two lamps is used. The first one is a deuterium lamp for the near UV-visible part and the second one is a halogen lamp for the visible part of the spectrum. The detection of the reflected light from the substrate/SiCN:H system is done with an AvaSpec-2048-USB2-RM spectrometer equipped with three CCD camera covering the near UV-IR spectral range.

The figure 2 shows an example of the measured reflectance at 600 nm extracted from the whole spectrum for the system Si/SiCN:H during the growth of the deposited film.

The pseudo-period τ of the reflectance signal can be calculated with a simple layer structure deposited on a thick substrate [31] and is given by the followed equation:

$$\tau = \frac{\lambda}{2 \cdot n_1 \cdot v \cdot \sqrt{1 - \left(\frac{\sin(\theta_0)}{n_1}\right)^2}} \quad (1)$$

where λ is the considered wavelength, n_1 the SiCN:H thin film optical index, v the growth rate and θ_0 the incidence angle. As it can be seen in figure 2, the pseudo period is affected by the product $n_1 v$ or $n_1 d$ where d is the deposited film thickness. If the pseudo-period is constant, the growth is considered homogenous. Thus, by measuring the thickness from the cross view of the SEM photographs, one can deduce the optical index n_1 of the thin film from equation (2) at the considered wavelength:

$$n_1 = \sqrt{\frac{\lambda^2}{4\tau^2v^2} + \sin(\theta_0)^2} \quad (2)$$

UV–visible spectroscopy (UV–Vis) analyses were performed with a double beam Varian Cary 5000 spectrometer in the 200–1100 nm range, for films deposited on quartz substrates (Suprasil ®) in order to determine their Tauc’s optical band gap according to Swanepoel work [32].

In the present work, we compare three plasma processes for SiCN:H thin films deposition in order to highlight the effect of dual plasma coupling. For all the processes, the gas mixture is Ar/N₂/Si(CH₃)₄. The samples preparation is summarized in table 3.

- The process A consists in using only the ECR plasma applicators, and varying the nitrogen content from 0 to 33% in the gas mixture. The Argon content was adjusted to maintain the total gas flow constant.
- The process B consists in studying the effect of the autopolarisation voltage V_{bias} of the silicon magnetron target in the rf MS mode, and fixing all other gas contributions to the deposition process.
- The process C consists in coupling the four ECR applicators with the rf MS plasma, named hereafter dual plasma. We will study the effect of the autopolarisation voltage V_{bias} on the properties of the obtained films, in order to highlight the potentialities of this PACVD process.

3 Results and discussion

3.1 Introduction

The OES lines observed are summarized in table 1. In the case of the ECR plasma (process A) when varying the amount of nitrogen in the gas mixture one can notice that the N₂ vibrational band head (at 337.1 nm) intensity increase quasi linearly with nitrogen addition (cf. figure 3a). A maximum of emission for NH and CN band head at about 6% of nitrogen in the gas composition (cf. figure 3b and 3c). The Ar lines (figure 3d) and hydrogen H_α (figure 3e) decrease. The Ar⁺ line (figure 3f) is weak and seems to be constant. Thus the electronic density probably remain constant, and the nitrogen injection in the plasma, lead to enhance the vibrational modes of nitrogen. The silicon emission line (cf. figure 3g) is very weak which is probably due to a diffuse plasma regarding the low total pressure and probably a poor dissociation of TMS. One should enhance the microwave plasma power but it is not possible with the ECR applicators used, due to limitation in peak power of 240 W. No oxygen or OH lines were observed with OES characterization.

The thickness of the thin films obtained in this conditions vary very slowly vs N₂ percentage in the gas mixture, and is about 50 nm. We have decided to fix the amount of nitrogen at 8% of the total flow for the following studies in order to limit the concentration of NH etching species, and CN as consequence of the etching of the surface and or the recompositing of radicals from the TMS dissociation. Subsequently we fixed the gas composition as follows: 8% N₂, 17% TMS, 75% Ar of the total flow for the study of the processes B and C in which we study the effect of the autopolarisation voltage V_{bias} of the magnetron cathode.

The anode is composed from the substrate holder and the vessel that is far from the magnetron cathode. The autopolarisation voltage of the magnetron cathode V_{bias} can thus be considered

proportional to the energy of the Ar^+ ions in the sheath around the rf magnetron cathode bombarding the silicon target. The variation of this voltage vs the applied rf power is presented in figure 4. One can notice a double linear behaviour, the slope changes at $V_{\text{bias}} \approx 75$ V that could be explained by the beginning of the efficiency of the silicon target sputtering.

The table 3 summarises the studied samples for the comparison of the processes B and C.

3.2 Morphology thickness and chemical composition of the thin films

In figure 5 is presented the measured thickness from cross view SEM photographs of the films obtained after 1 h deposition in the processes B and C vs the V_{bias} voltage. One can notice how the thickness and thus the growth rate is expanded by a factor around 40 and reaches a huge value of about 0.6 nm/s at $V_{\text{bias}} \approx 200$ V for the processes B and C, compared to the low growth rate of about 0.014 nm/s obtained for the process A. The enhancement in the growth rate became particularly noticeable when the sputtering of the silicon cathode became effective at $V_{\text{bias}} \approx 75$ V.

In figure 6, are presented the HRTEM results obtained for the sample deposited at $V_{\text{bias}} = 150$ V with the process B (fig. 6a), and C (fig. 6b). In fig. 6a, the images correspond to X maps and EDS (left), TEM (right and top down) from FIB slices. The chemical composition seems relatively homogenous for the elements N, C, Si and O. A contamination of the sample interface is observed with the presence of elements Ca and S. It corresponds probably to CaSO_4 . This contamination probably comes from a cleaning pad used for the vessel cleaning. The presence of Oxygen is due to post oxidation of the sample when the reactor is vented. This was observed for many processes used for SiCN:H thin films synthesis and it's due to the porosity of the films favoring a slow oxidation mechanism [10, 12, 33-35, 44]. The bird feather like structure is due to the contamination that favors the growth of this amorphous structure. Electron diffraction measurement on the selected area indicate an amorphous structure of the deposited

film. The HRTEM photograph indicate that the interface between the sample and the film is about 10 nm.

The figure 6b shows EDS (left), HRTEM (top right) from FIB slices and SEM front view (right down) for the sample obtained at $V_{\text{bias}}=150$ V with the process C. One can notice the homogeneous composition in the elements C, Si, N and O. No pollution is observed in this case. The electronic diffraction indicate that the film is amorphous. The excess in C element at the top surface comes from the polymer deposited for FIB slices preparation. The excess in O is due to the porosity in the film inducing a post oxidation after the release to the air. This very slow oxidation process have been studied with time resolved FTIR measurements for similar films [33]. The mechanism of oxidation could be due to Oxygen incorporation and changing bonds that have been organized during deposition of the film. It could be due to silicon atoms dangling bonds, or H termination bonds making an exchange of SiN bonds to SiO ones, with air/oxygen exposition. Recently, Chagin *et al* [35] have shown the stability of such films when the oxidation mechanism is finished after about 100 h in air. The HRTEM micrograph exhibit a clear interface of about 10 nm between the silicon substrate and the amorphous deposited film. The film have an orange skin like structure, and it's surface is very smooth as we can see on the SEM micrograph. The same phenomenon of oxidation was observed when the WSiC:H samples deposited in similar plasma reactor with the same dual plasma excitation and annealed in air at 500°C [17].

3.3 Optical characterisation of the plasma and the thin films

the OES results concerning the process A were presented in §3.1 in fig. 3. The OES characterization of the plasmas for processes B and C is discussed in the following. All the observed lines according to table 1 increase quasi linearly with V_{bias} . A small shift is observed

for all the emitting lines according to table 1 in the case of process B or C when the sputtering of the silicon cathode occurs. An illustration is presented for silicon emission line in figure 7a. The emission of atomic silicon line is very weak for V_{bias} lower than about 75V for the two processes. Then it is highly enhanced when the sputtering of the silicon target is effective for $V_{\text{bias}} \approx 75\text{V}$ for the two processes. For H_{α} line (cf. figure 7b), we observe the same behavior, with a very low emission of H_{α} line under about 60V, and an quasi linear increase up to 100V, then a small shift corresponding to a change in the matching box of the RF generator. In the case of process C, a quasi linear increase is obtained then a saturation is observed at $V_{\text{bias}} \approx 175\text{ V}$. For this process, we observe the same saturation for the NH, N_2 and CN lines (cf. supplementary data figure 1 for process B, and figure 2 for process C) at $V_{\text{bias}} \approx 175\text{ V}$. The shift in the intensity between the same emitted line for the two processes could be due to a small displacement of the optical fiber between the two measurements. Ar^+ lines augment with V_{bias} for the two processes indicating an increase in electronic density as observed in [34].

The two processes B and C are different in terms of plasma reactivity, electronic temperature and electronic density, and also the silicon cathode oxidation when the plasma chamber is opened. The saturation of the lines for the process C could be explained by a limit of TMS dissociation when the amount of atomic silicon attain a certain density in the plasma volume or a change in the automatic matching box of the RF generator that could limit silicon sputtering. In case of process B, this limitation is not obtained for $V_{\text{bias}} \approx 175\text{ V}$, and could saturate for V_{bias} higher values that we can't obtain with the RF generator [34]. The increase of V_{bias} lead to more atomic silicon in the plasma, a better dissociation of TMS illustrated by H_{α} increase, due to an increase of electronic density. The increase of CN, and NH lines can also be explained by the increase of electronic density.

For the processes B and C, the growth rate vs V_{bias} (figure 5) have the same behavior indicating that the plasma reactivity goes to the deposition predominance instead of etching. The clusters

formed in the plasma volume are more beneficial for the growth, and their size is an image of what we observe on HRTEM photographs on figure 6 (a and b). The presence of atomic silicon in the plasma volume augments the TMS dissociation by the augmentation of electronic density. Thus it favors the agglomeration of radicals on both the sample surface or the plasma volume and favors the growth rate.

The work of Chagin *et al* [35] gives a high value of the electronic density in an ICP plasma that we can consider similar to our dual plasma, even if the pressure is 10 times lower in their case. They give an electronic density of $n_e \approx 2 \times 10^{12} \text{ cm}^{-3}$. This high value indicates the good reactivity of such plasma, in terms of TMS dissociation and radicals creation inducing a high chemical reactivity of the case of dual plasma.

UV-visible spectrometry of samples corresponding to the three processes are presented in figure 8a. One can notice that the sample corresponding to the process A is transparent in the near UV range and small oscillations are obtained in the transmittance due to its very low thickness ($\sim 50 \text{ nm}$). More important oscillations are obtained for the samples from B and C processes due to the increase in the thickness and optical index variation.

In figure 8b is plotted the transmittance at 300 nm vs V_{bias} for the three processes. The films corresponding to the B process are opaque in the near UV range. One can notice that even when the V_{bias} is around 50V, the UV transmittance is decreased to 27.5%. Some of the films corresponding to the C process are transparent at the wavelength of 300 nm and an acceptable value of 83% is obtained for $V_{\text{bias}} \approx 100 \text{ V}$, then an important decrease is observed.

The transmittance is affected by the film thickness, but also by the used plasma process inducing a difference in film composition and particularly hydrogen content in the film inducing a difference in the optical index.

The reflectometry signal in case of processes B and C is regular as presented in figure 2. In this case, we use it to determine the optical index at a given wavelength from equation (2). In figure 9 one can notice the quasi-linearity of the pseudo-frequency of the signal vs the V_{bias} voltage at 600 nm. This indicates that we have the similar growth mechanism when V_{bias} vary. The simple layer optical model we have used for the optical index calculation can thus be considered acceptable in regard to the high thickness and optical index of the films obtained for B and C processes. The calculated optical index from equation (2) at 633 nm is plot vs the V_{bias} voltage in figure 10. In the same figure is plot the calculated Tauc's band gap extracted from UV-vis absorption spectroscopy spectra [32]. We assume the indirect character of this parameter according to the literature [8, 12-13, 15, 17, 24, 35]. One can notice that for the process B, a very slow variation in the optical index from 1.8 to 1.9 and in regard to the reflectometry limitations and the calculation model, it can be considered quasi-constant. The Tauc's band gap for the samples of process B is also considered quasi-constant. In the case of the process C, a large linear variation in the optical index and the band gap is obtained. This results make the process C very versatile opening large possibilities in optical applications. One of them could be the growth of thin films with gradient optical parameters. Recently Szymanowski *et al* published results on gradient optical index SiCN/SiOC by varying the ratio between O_2 and N_2 in the gas mixture [36]. They present results for the optical index that are coherent with those obtained with spectroscopic ellipsometry [12-13, 15, 17, 19, 34]. Our in-situ reflectometry results obtained with this simple equipment and optical model give credible results.

Because of the small thickness of about 50 nm obtained with the process A for 1 h deposition time, we have carried out a deposition for 7 h in the same gas mixture used for processes B and C (8% N_2 , 17% TMS, 75% Ar).

The figure 11a shows the EDS chemical composition (top left), the HRTEM photograph (top right) and the SEM cross view (down left) and front view (down right). The sample exhibit nanocolumns with a high aspect ratio (about 1 μ m height, 50 nm width). The chemical composition is homogenous in the columns, and voids are present in all elements distribution. The density of columns is constant on all the sample observed surface. The excess of carbon on the top of the sample surface comes from the polymer deposited for the FIB slices preparation, and a part of the polymer diffuses around the columns. The oxygen contribution is homogenous along each column indicating a porosity along each column itself. The oxidation mechanism suggested for B and C processes is probably the same in the case of process A with a faster kinetic in this case in regard to the expanding of the area of the sample. Regarding the elements composition from EDS measurements and the HRTEM photograph, the composition seems to be homogeneous in each column. The reflectometry signal is shown in figure 11b. The reflectance is not periodic, and three different pseudo periods are obtained. The first one correspond to an incubation period and it takes about 3h, but it do not correspond to the moment of the apparition of the nanocolumns. It depends on the wavelength selected for the extraction of the reflectometry signal. The attenuation of the signal could be due to the incidence angle of 45° used in our experiment, or a small displacement of the optical fiber during the experiment. The second and third pseudo period are about 1.5 h and correspond to the normal growth.

The UV-vis spectrum of the this sample is presented in figure 11c and compared to the one obtained for 1 h deposition time. The indirect band gap is about 5 eV for the 7h deposition sample indicating a silicon nitride type for this sample. The transmittance remain important in the visible range.

The growth of nanocolumns could not be observed for the samples from processes B and C. These two processes correspond to a huge kinetic growth. The etching species do not have the

same effectiveness compared to the case of ECR plasma (process A). The 2D growth is favoured thanks to silicon sputtering in processes B or C. The incubation time in case of B and C processes is really very short, ~~and takes few minutes~~ depending on the V_{bias} value.

3.4 FTIR analysis of the thin films

FTIR spectroscopy examinations provide information on the chemical bonds and groups contributing to the film bulk structure. Bonding in the volume of the film are probed through IR absorbance spectra obtained in transmission mode.

Raw FTIR spectra contain oscillations due to interferences of the IR beam in the thin film. We have developed a software ASUVIR [33-34] based on the work of Milosevic *et al.*[37-38] and Peter *et al* [15] permitting to extract the oscillating baseline from the raw spectrum. The correct oscillating baseline should give the sample thickness and its optical index in the IR. We consider that this determination of the oscillating baseline is correct when the thickness is in concordance to the one obtained from SEM measurements and the IR optical index is correct in regard to the value obtained from reflectometry measurements in the visible range. Thus, the deconvolution of the FTIR spectra is more accurate and permit to extract the density of each bonding present in the film by normalizing the corrected spectrum to the film thickness, permitting to compare the films obtained with the processes A, B and C.

In figure 12a we present the raw FTIR spectrum obtained for process A (7h deposition), and the calculated oscillating baseline. In the same figure is presented the corrected spectrum with a reference line equal to zero for the all spectrum. The deconvolution of the fingerprint region is thus conducted for the fingerprint IR domain between 400 and 1400 cm^{-1} by considering a Gaussian shape of each oscillator as summarised in the table 2. The fingerprint deconvolution

is presented in the box of figure 12a. In many papers authors consider more contributions corresponding to asymmetric and symmetric stretching and bending modes [9, 12, 15, 20, 21, 30, 35, 36]. For the sake of simplification we wish above all to go back to the chemical composition, and consider a bond contribution without details of contribution of type of modes, and consider the bands presented in table 2, these considerations permit the deconvolution with low number of gaussian functions as presented in the box of figure 12a. The SiC contribution maximum is around 850 cm^{-1} , the SiN maximum contribution is around 950 cm^{-1} , the SiO contribution is around 1050 cm^{-1} , and SiCH₃ is around 1200 cm^{-1} .

The difference in the three processes of SiCN:H thin film deposition is highlighted in the figure 12b in which is displayed the fingerprint region ($600\text{-}1300\text{ cm}^{-1}$). The process A gives films with a rich signature of SiO and SiN contribution, SiC is very low. The films obtained with processes B and C gives contributions of SiC, SiN, SiH, NH...bonds.

The results of the deconvolution of the fingerprint area of the samples obtained with process A (1h deposition) when N₂ percentage vary in the gas mixture are not presented because of the very small thickness of the films, the variation of contributions is not significative.

In case of process B, the deconvolution of the fingerprint domain gives an increase in SiN, SiO, SiC density of bonds vs V_{bias} (cf. figure 13a). The adjunction of atomic silicon in the gas mixture from the sputtered silicon target permit the consumption of the other species present in the plasma, particularly nitrogen, and carbon radicals coming from the TMS dissociation. The presence of oxygen in the volume of the samples illustrated by SiO linking comes from an oxidation of rich surface silicon dangling bonds. Thus, depending on the porosity of the deposited film, oxidation can occur in the volume. SiCH₃ density of linking is constant and can be considered as an image of TMS dissociation in the process. It remain constant for all the samples obtained with the process B. The films seems to became denser with atomic silicon adjunction.

In case of process C (see figure 13b), the density of linking of SiC increase with V_{bias} . The reactivity of the dual plasma seems to give more dissociation of the TMS inducing the observed increase in SiC density of linking with V_{bias} . The carbon in the thin film comes from TMS dissociation, and could be in the form of methyl CH_3 , CH_2 , CH radicals or atomic carbon depending on the chemical reactions occurring in TMS dissociation. This fact can be highlighted by the obtained results in UV-visible spectroscopy (figure 10) where the obtained film for high values of V_{bias} exhibit an optical bandgap corresponding to SiC:H like structure as reported in the literature for SiCN:H with an optical behaviour like SiC:H thin films [12-15], but in our case we have highly modified the ratio between silicon and carbon in the gas mixture. This was also reported by Lavareda *et al* [39] when depositing SiCN:H thin films in RF capacitive plasma with $\text{SiH}_4/\text{CH}_4/\text{NH}_3$ gas mixture.

In figure 14, we have plot the evolution of density of bonds corresponding to SiH (figure 14a and 14c) and NH (Figure 14b and 14d) for samples obtained respectively with process B and C. In figure 14a one can notice that the spectra are not symmetric, and the deconvolution could give two contributions corresponding to SiH_2 at 2125 cm^{-1} and SiH at 2175 cm^{-1} . The maximum for $V_{\text{bias}}=50, 100$ and 200 V is about 2175 cm^{-1} , whereas for $V_{\text{bias}}=150\text{V}$, the maximum is at about 2190 cm^{-1} . The contribution of the SiH_2 density of bonds for samples obtained under $V_{\text{bias}}=100\text{V}$ seems higher than SiH contribution. For $V_{\text{bias}}>100\text{V}$, the opposite situation could be observed. This could be explained by the more presence of atomic silicon in the gas phase limiting the SiH_2 bonds formation in the film, because the amount of hydrogen in the gas mixture do not change and is fixed by the TMS source of hydrogen.

In case of figure 14b, the density of bonds corresponding to NH do not vary very much. This could be explained by the fact that the ratio between N and H in the gas mixture is the same for all experimental conditions and only the silicon contribution change, but the affinity of nitrogen to hydrogen is better than the one of silicon to hydrogen. The maximum of the NH

contribution is about 3355 cm^{-1} for $V_{\text{bias}}=100, 150$ and 200 V , whereas it's at about 3365 cm^{-1} for $V_{\text{bias}}=50\text{V}$. A small contribution of OH bonds is observed for all the samples depending on the moisture in the experimental room, which was not correctly eliminated in the calibration procedure. In figure 14c one can notice that the sample obtained at $V_{\text{bias}}=200\text{ V}$, represent the lowest density of SiH bonds. This is probably due to the automated matching network of the magnetron cathode which is not totally adapted in impedance in this case. One can observe a small shifting of the maximum at about 2250 cm^{-1} for the samples obtained with $V_{\text{bias}}>100\text{ V}$ compared to those obtained at lower V_{bias} . Silicon environment in the thin film change when V_{bias} augment, and thus SiH₂ contribution at 2275 cm^{-1} [30]. In figure 14d, the samples corresponding to $V_{\text{bias}}=175$ and 200 V exhibits a small contribution of OH at about 3550 cm^{-1} . All the obtained bands are asymmetric indicating that another contribution appears at lower wavenumber. This could be a contribution of NH₂ at about 3300 cm^{-1} . In our case the maximum shifts from 3380 cm^{-1} for the sample obtained at $V_{\text{bias}}=50\text{V}$ to 3350 cm^{-1} for the sample obtained at $V_{\text{bias}}=175\text{ V}$. The chemical environment of NH bonding change with V_{bias} , due to atomic silicon presence in the plasma and incorporation in the film inducing a change in the film density.

3.5 Discussion

According to the work of de Poucques *et al* [40] on spatial characterization of an ionized physical vapour deposition (IPVD) reactor using a Ti magnetron target with Argon gas and an additional microwave plasma. At about 10 cm from the magnetron target, the ratio between neutral and ions is about 100. Furthermore, Chagin *et al* [35] found an electronic density $n_e \approx 2 \times 10^{12}\text{ cm}^{-3}$ and the electronic temperature $T_e \approx 3\text{ eV}$ in their ICP plasma used for SiCN:H

thin films deposition. If we assume that this kind of plasma coupling is similar to our dual plasma in terms of electronic density and temperature. One can consider that in our dual plasma discharge, essentially silicon neutrals coming from the silicon cathode and TMS radicals contribute to the SiCN:H film formation. This results will be a guidance to the interpretation of our results from OES measurements. The substrate holder in our experiments is grounded, and no Ar implantation in the films was observed contrary to Peter *et al* [41] who have observed Ar incorporation into the SiCN:H obtained in ECR plasma by XPS measurements.

In case of process A with only ECR plasma excitation, it appears that the silicon emission is very weak, probably because the plasma is very diffuse, and the ECR effect is essentially around the applicators, then the plasma diffuse to the chamber volume and the dissociation of the TMS precursor is low. However, the CN, NH and H α emission lines or bands are present inducing a certain degree of dissociation of TMS. This can be due to different effective section of this radicals and atoms. The choice of 8% percentage of nitrogen in the feed gas can be justified by the proximity of the maximum observed for CN and NH bands at about 6% of nitrogen in the feed gas, corresponding to the maximum of the ECR plasma reactivity. 8% appears as a good compromise for TMS dissociation, and slower emission variation of NH and CN, with an acceptable value of H α emission (cf. figure 3).

In case of process B corresponding to a magnetron RF plasma excitation, the effective sputtering of the silicon cathode occurs at about an autopolarisation voltage $V_{\text{bias}} \approx 75\text{V}$, permitting the observation of a good signal of silicon emission line. In this case, it corresponds mainly to atomic silicon sputtering from the cathode [40]. Silicon from TMS, participate to the discharge emission (figure 7 and supplementary data figure 1), which is lower under $V_{\text{bias}} \approx 75\text{V}$, but its contribution became low in regard to the silicon from the sputtered cathode. All the other lines and bands of table 1 increase with V_{bias} inducing a better reactivity when the sputtering of the cathode became effective. This could be due to an increase in the electronic density as

we observed for Ar⁺ line, and probably electronic temperature. We have more electrons in the discharge, thus TMS dissociation is more efficient by electronic collisions and induce more CN, NH, H_α, Ar, Ar⁺...emission.

For the process C corresponding the dual ECR plasma/RF magnetron plasma, the same behaviour of the emitted lines and bands is observed (figure 7 and supplementary data figure 2). A small plateau is observed for V_{bias}=175V. This could be due to a limitation with the automated matching network of the magnetron cathode.

The clusters formation in such processes seems to give a very smoother surface in the case of B and C processes. In similar work in an ICP plasma discharge Bang *et al* [42] have found in the Ar/SiH₄/O₂/N₂ gas mixture that the aggregation of spherical nanoparticles depends on the gas composition and RF power inducing different porosity in the barrier SiON and the crystallinity of nanoparticles collected on the film surface for TEM analysis. In our case, the process C seems to limit the clusters aggregation inducing the orange skin like surface at the atomic scale as we observed in figure 6b.

Annealing of the films was not conducted in this study. This can affect the chemical composition of the films, inducing a change in their optical and mechanical behaviour as presented in [17-43].

The obtained values of the refractive index from *in-situ* Reflectometry in case of process B and C are acceptable considering the large published results in the literature obtained with spectroscopic ellipsometry in this field of SiCN:H thin film plasma synthesis.

In the case of process A where the growth rate is very low, the reflectometry results give an idea about incubation time regarding the wavelength chosen to extract the signal. The process A permit to obtains nanocolumns growth that exhibit high aspect ratio. In the case of 7 h

deposition, the columns have 1 μm height and 50 nm in diameter. The films are transparent in a wide part of the measured spectrum from near UV to near IR.

In case of process B, V_{bias} plays an important role in the growth rate that can be about 40 times higher than the one obtained with process A. The chemical composition of the films change with V_{bias} (fig. 13a), but this variation induce small consequence on the optical parameters (fig. 8b and 10). The films obtained at $V_{\text{bias}} > 100$ V are not transparent in the near UV. This could make them attractive for use as optical filters.

The Process C appears very attractive. The combination of many ECR plasma applicators and a rf magnetron plasma permit to obtain near UV transparent films for $V_{\text{bias}} < 75$ V with an acceptable growth rate for many applications. The high growth rate obtained with this process is similar to the ones obtained for process B. Very large modulation of the optical parameters can be obtained depending on atomic silicon incorporation in the dual plasma discharge and hydrogen content. Similar modulation of the optical parameters was obtained in a RF magnetron discharge in $\text{CH}_4/\text{N}_2/\text{Ar}$ with silicon target [44]. In this case the increase of the relative N_2 flow rate induce a diminution of XH density of bonds ($X = \text{Si}$, or C), and affect the optical parameters. The C process could be largely used for gradient optical index thin films deposition by varying the V_{bias} voltage gradually during the process. This could give more possibilities than changing the gas composition during the growth as proposed in [36]. The combination of the two processes A and C could lead to the obtention of multi-layered thin film with the right porosity, that could promote SiCN:H thin films associated to an oxide catalyst in the photoelectrochemical water splitting and hydrogen production as recently proposed in the review of Jian *et al* [45] where potentialities of SiC materials are highlighted. An other potentiality was recently published by Diop *et al* [17] in cermet SiC:H-W cermet synthesis in dual plasma for solar concentrators thin films.

The opportunity to grow a design material with adequate optical parameters and number of layers or gradient of optical parameters is largely possible with the dual ECR/Magnetron plasma by choosing the adequate organometallic and magnetron cathode compounds.

The inconvenient of these processes is to produce porous films from high aspect ratio nanocolumns in case of process A, to very small pores in case of process B and C, and one can recommend to add oxygen in the gas phase, in order to stabilise the films rather than annealing after deposition in order to make them suitable for many applications.

4 Conclusion

We have compared three low pressure PACVD processes for the synthesis of SiCN:H thin films in Ar/N₂/Si(CH₃)₄ gas mixture.

The ECR plasma gives a very low growth rate, and for high deposition time, columnar SiCN:H structures with high aspect ratio are obtained. The incubation time could take more than 1h in the operating conditions.

The synthesis in RF magnetron plasma with a silicon target permits to enhance largely the growth rate to a factor about 40 for an autopolarisation voltage of the magnetron cathode of $V_{\text{bias}}=200$ V. The obtained films are not transparent in the near UV range. The chemical composition do not vary to much in the operating conditions, leading to an optical bandgap of about 3.0 eV and an optical index at 633 nm of about 1.95.

The dual PACVD process combining ECR and RF magnetron plasma appears as a very promising deposition process. The growth rate could attain a high value of about 0.61 nm/s at $V_{\text{bias}}=200$ V. The chemical composition of the obtained thin films vary from SiC:H to SiN:H like regarding their optical properties. The bandgap take values between 4.75 and 3.4 eV and the optical index vary between 1.7 and 2.05 with the V_{bias} increase.

This versatility makes this process very suitable in many fields of low pressure thin films synthesis, particularly composites, catalysis... by changing the organometallic and magnetron cathode compound.

Declaration of competing interest

The authors declare that they have no known competing financial interests or personal relationships that could have appeared to influence the work reported in this paper.

Sample credit author statement

Dr. Robert Hugon: phd supervision, Conceptualization, Methodology, Software, Original draft preparation ; Dr. Ziad Al Hallak.: phd student, Samples preparation, Process control, data analysis, writing ; Dr. Ahmad Ahmad : phd supervision ; Pr. Adnan Naja: phd supervision; Pr. Thierry Belmonte: Reviewing and editing, search for funding ; Pr. Mohammed Belmahi : phd supervision, conceptualization, original draft preparation, writing; reviewing and editing, search for funding.

Acknowledgements

SEM, and UV-vis spectroscopy measurements are done in common services of IJL laboratory. Many thanks to our colleagues in charge of these equipment for their help and readiness, particularly Sylvie Migot and Jaafar Ghanbaja respectively for FIB samples preparation and HRTEM measurements. Many Thanks to Dr. P. Pigeat for fruitful discussions on reflectometry measurements and Dr. G. Henrion for scientific discussions.

This work was partly funded by the “Agence Nationale de la Recherche” the French National Research Agency (Project HD-Plasm-A-SiNOC:H in association with four laboratories PROMES-Perpignan/IMN-Nantes/ICCF-Clermont-Ferrand/IJL-Nancy FRANCE). Many Thanks to all colleagues involved in this project and fruitful discussions.

This project was also partly funded by the French ICEEL Carnot Agency (Ultradur Project).

List of figure captions

Figure 1: Schematic view of plasma deposition reactor: a) top view, b) side view including the optical set-up for in-situ reflectometry measurements.

Figure 2: Example of Si/SiCN :H system reflectance vs time obtained from in-situ reflectometry measurements for an incidence angle $\theta_0=45^\circ$ and a wavelength $\lambda=633$ nm.

Figure 3: OES lines variation vs nitrogen percentage in ECR plasma discharge (Process A): (a) band head of N_2 at 337.1 nm, (b) band head NH at 336 nm, (c) band head of CN at 388.3 nm, (d) Ar line at 811 nm, (e) H_α line at 656.3 nm, (f) Ar^+ line at 472.6 nm, and (g) Si I line at 288.1 nm.

Figure 4: Autopolarisation voltage V_{bias} vs applied RF power to the Si magnetron cathode in the case of process B (see table 3). The solid line is a guide to the eye.

Figure 5: Thickness of SiCN:H thin films, obtained after 1h of plasma deposition vs autopolarisation voltage V_{bias} for the three processes.

Figure 6: EDS, HRTEM and SEM measurements of some samples illustrating the processes B (a) and C (b).

Figure 7: (a) OES Si line (see table 1) vs V_{bias} for the three processes A, B and C (see table 3). (b) H_α line at 656.3 nm for the processes B and C (and supplementary data).

Figure 8: (a) UV-visible spectroscopy transmission spectra for some SiCN:H samples corresponding to the processes A, B and C. (b) Transmittance at 300 nm vs V_{bias} for the three processes.

Figure 9: Evolution of pseudo-frequency obtained from reflectometry measurements at $\lambda=600$ nm for the processes B and C.

Figure 10: Tauc's optical bandgap, and optical index at 633 nm vs V_{bias} for the processes B and C. The dashed lines correspond to a linear fit for the Tauc's bandgap and the optical index.

Figure 11: Sample obtained with Process A after 7 h deposition time (a) EDS, HRTEM and SEM measurements, (b) reflectometry signal at 600 nm, (c) UV-visible spectrometry spectra for samples corresponding to 1 and 7 h deposition time.

Figure 12 : (a) raw FTIR spectrum for the sample obtained with process A (7h deposition), calculation of the oscillating base line, and corrected spectrum. The inset is the deconvolution of the fingerprint.(b) Fingerprint domain of some significant samples obtained with the processes A, B and C vs V_{bias} .

Figure 13: FTIR finger print deconvolution according to table 3, (a) Process B and (b) Process C. The dashed line is a guide to the eye for SiC contribution in process C.

Figure 14: Variation of linking density vs V_{bias} in processes B and C according to table 3. (a and c) SiH stretching band respectively for processes B and C, (b and d) NH stretching band respectively for processes B and C.

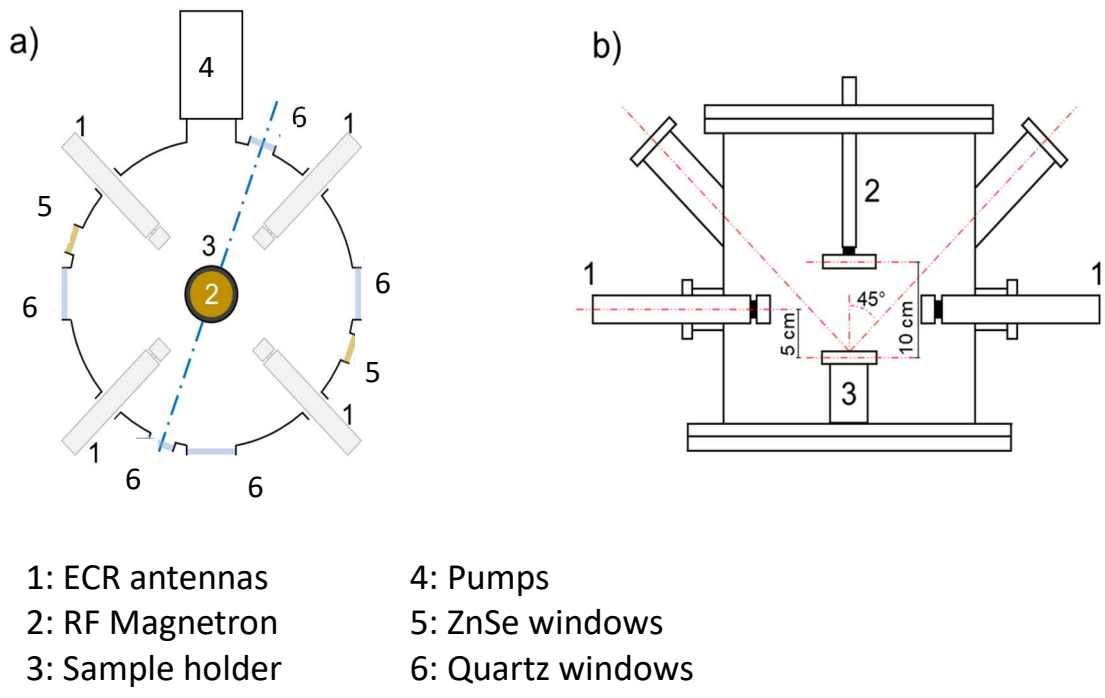


Figure 1

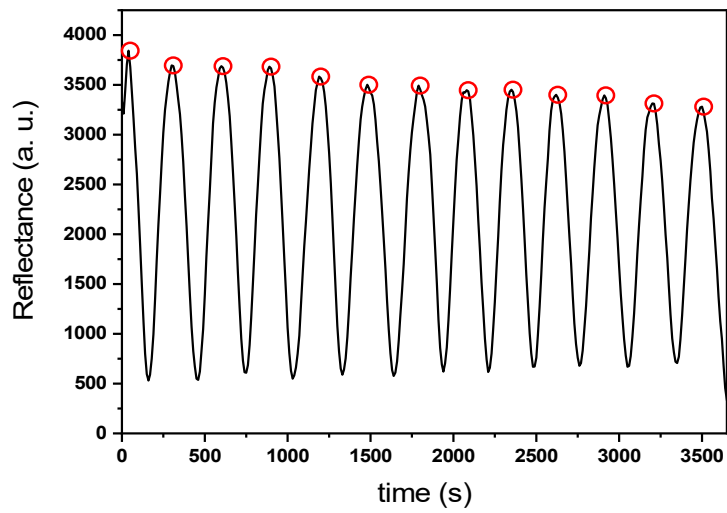


Figure 2

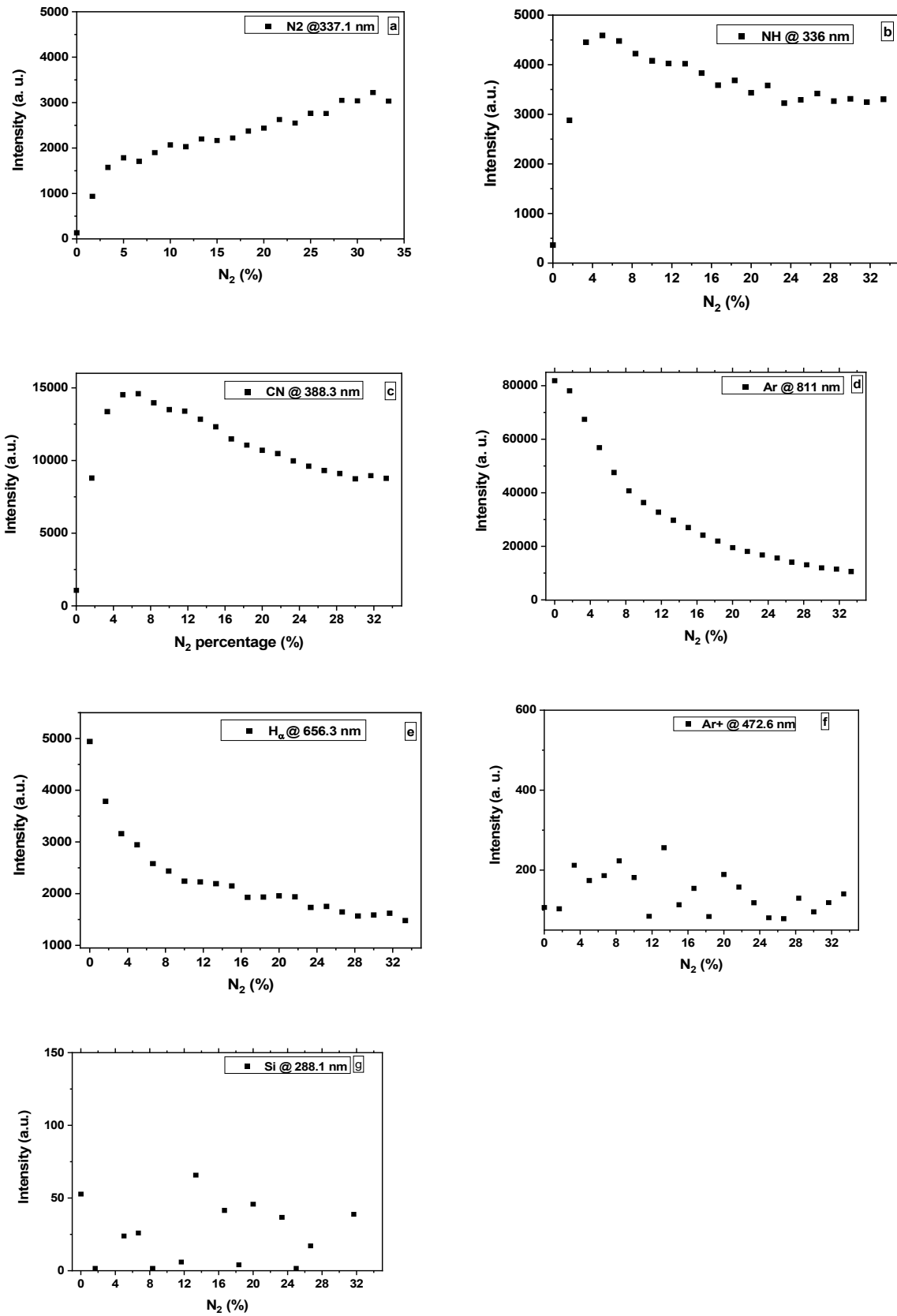


Figure 3

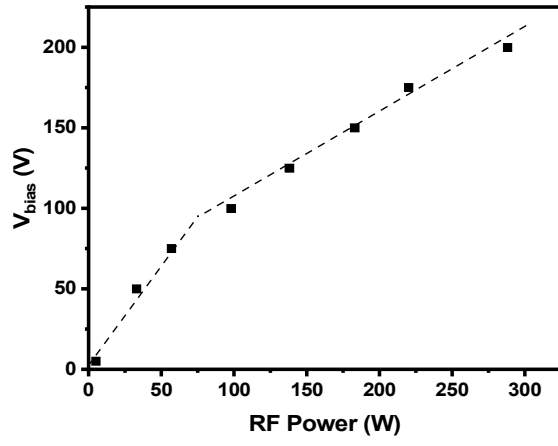


Figure 4

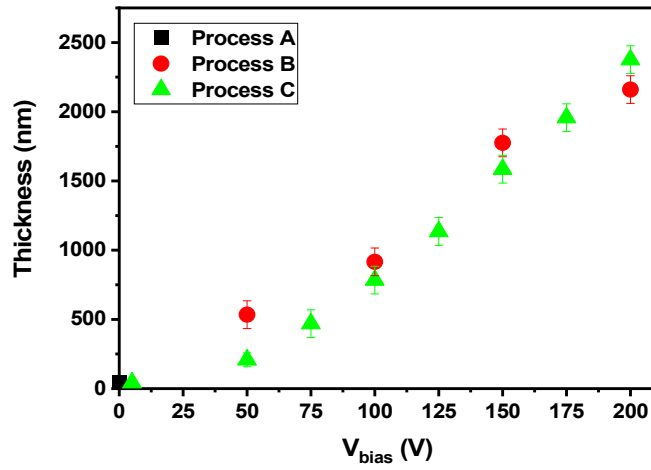
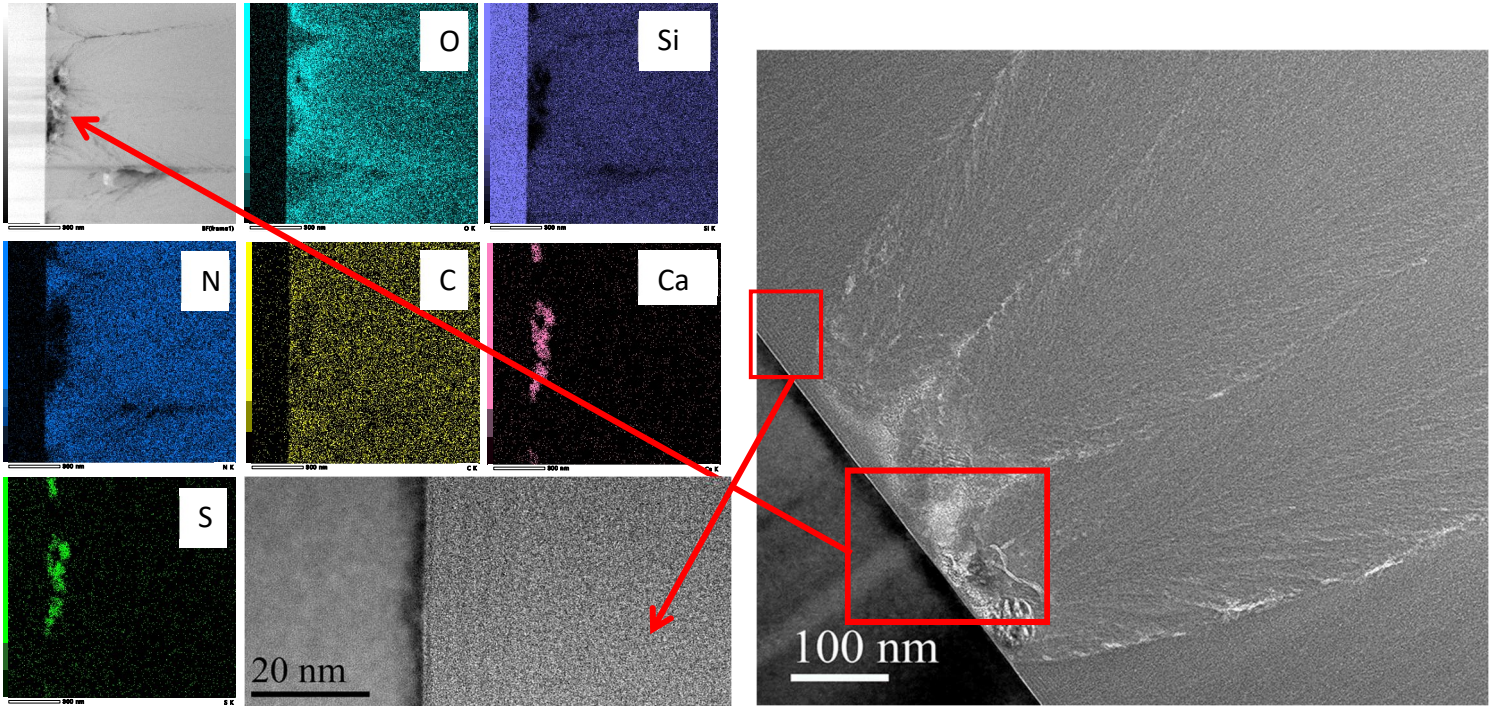


Figure 5

Process B (a)



Process C (b)

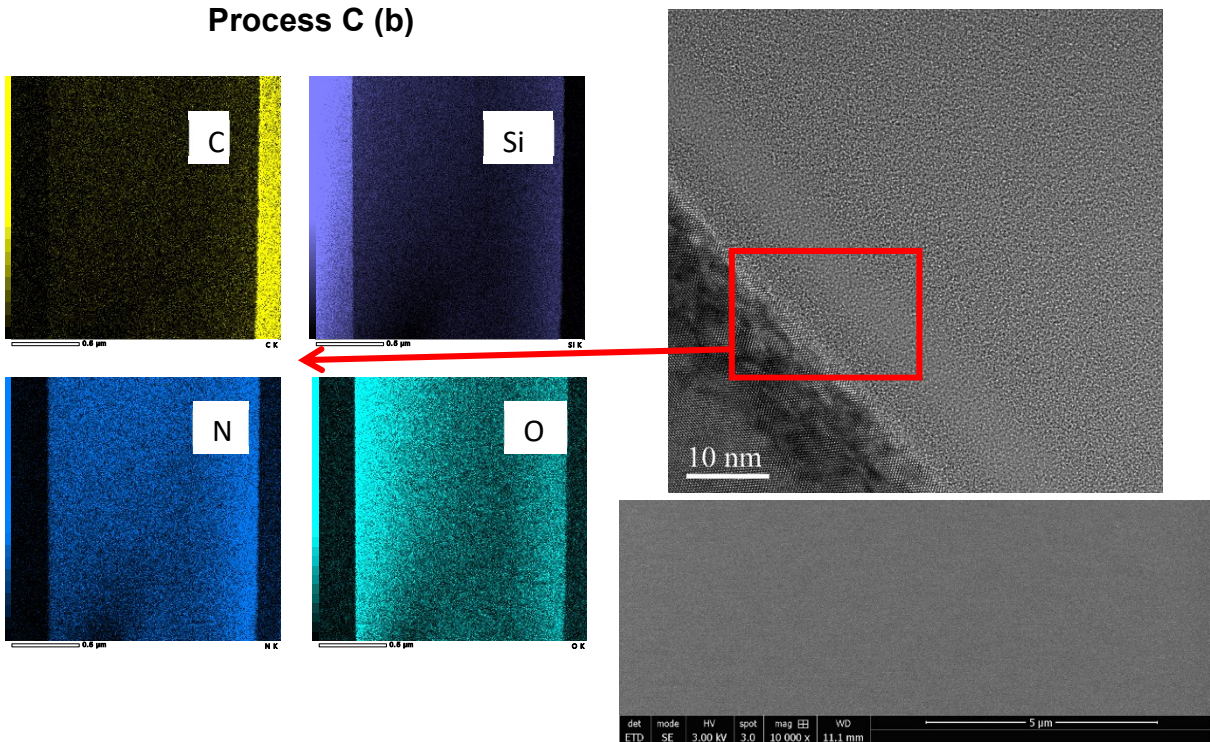


Figure 6

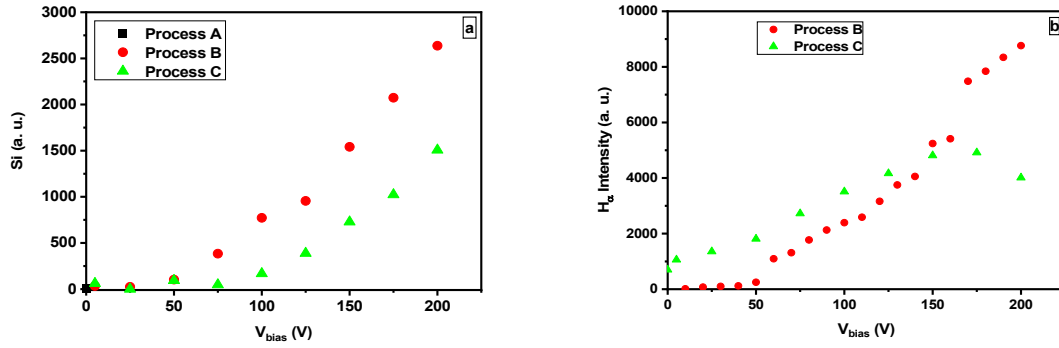


Figure 7

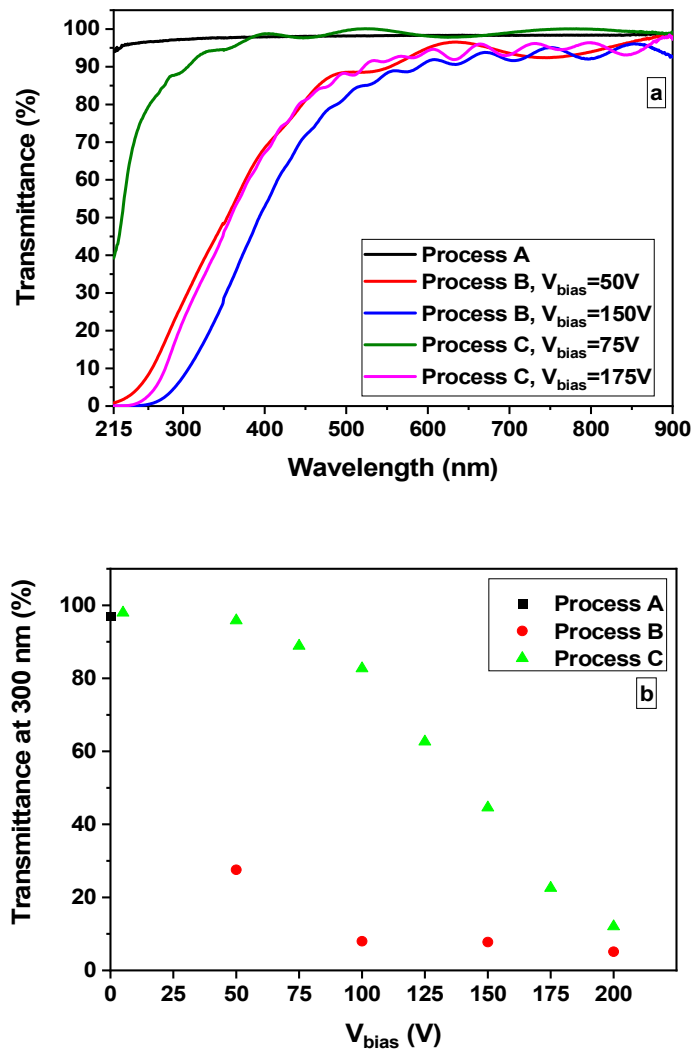


Figure 8

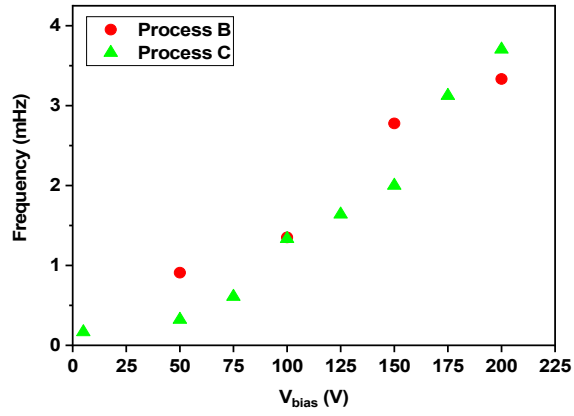


Figure 9

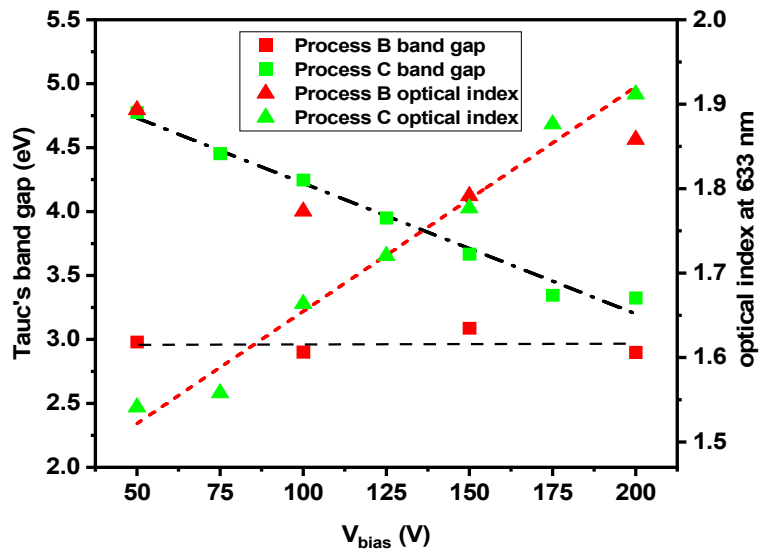


Figure 10

Process A

a

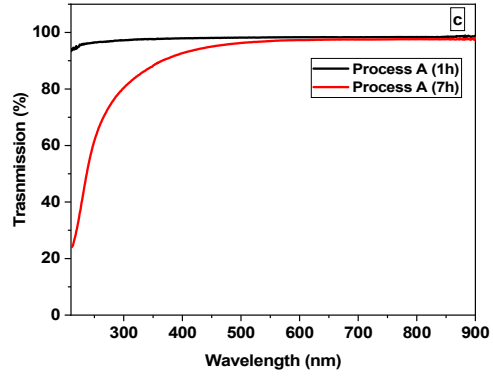
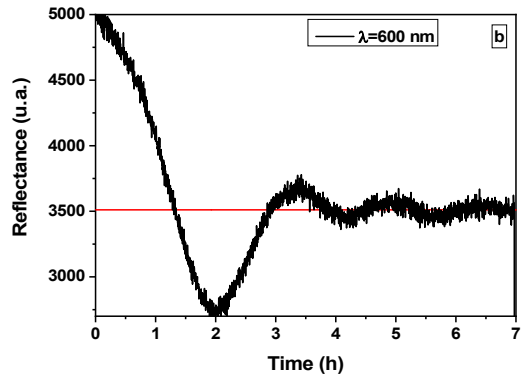
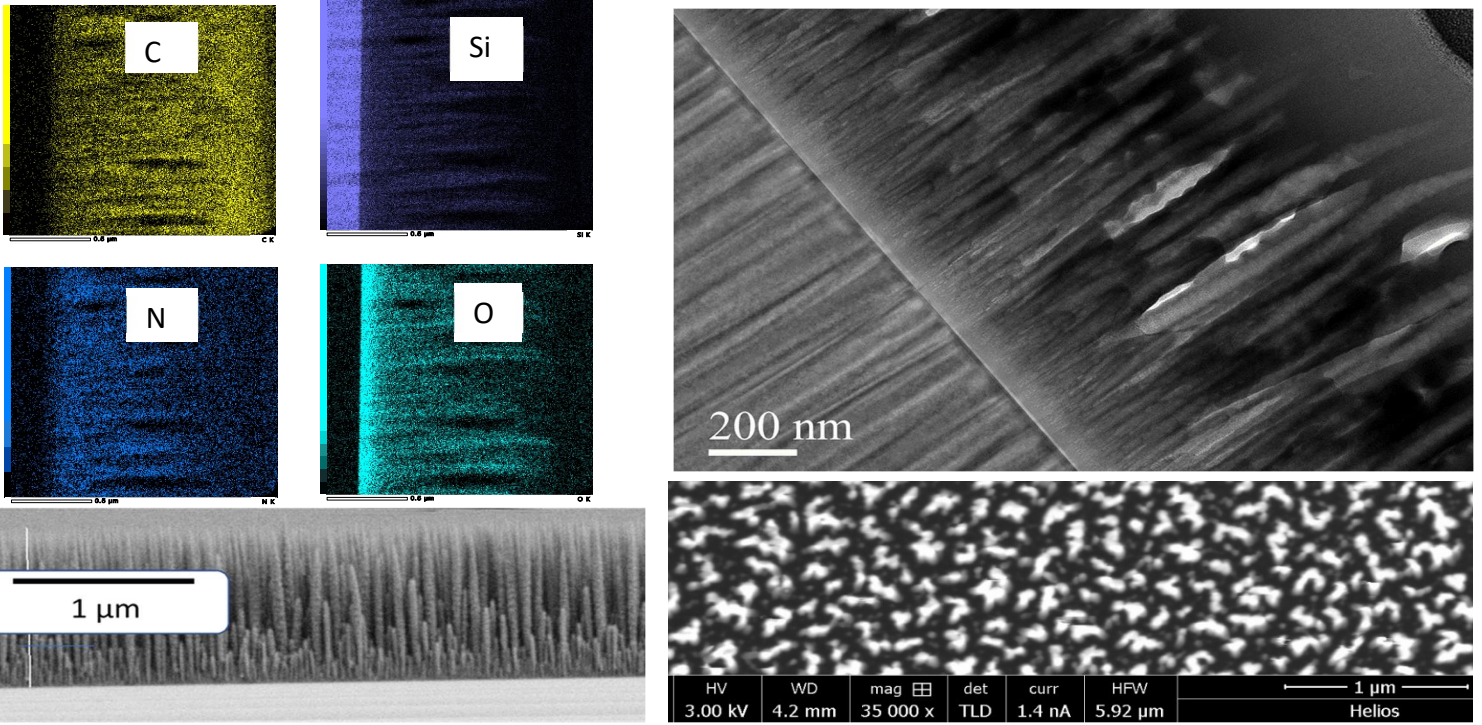


Figure 11

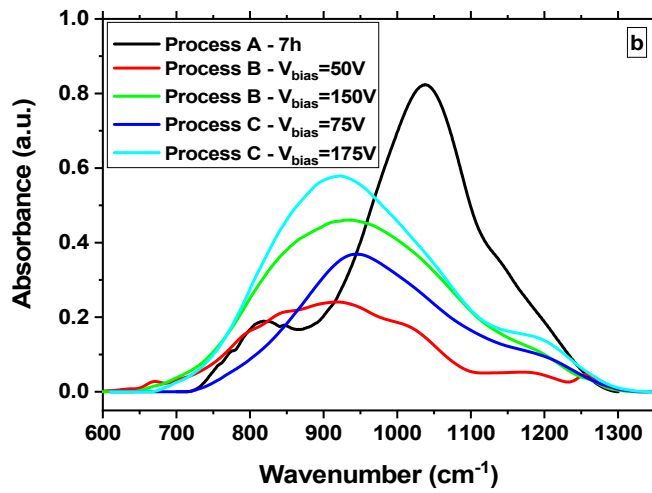
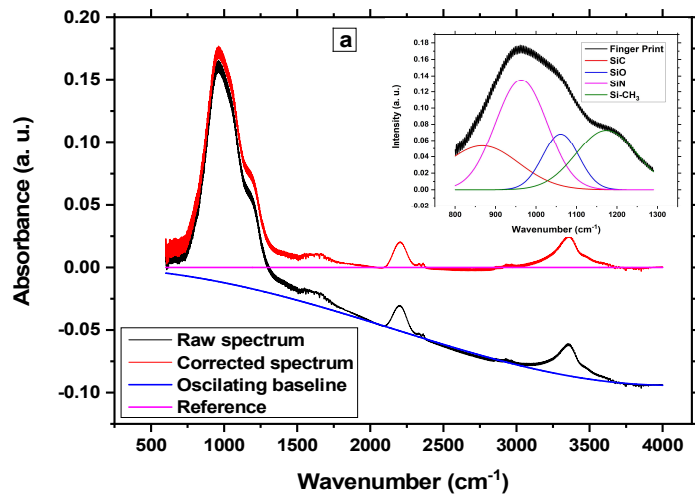


Figure 12

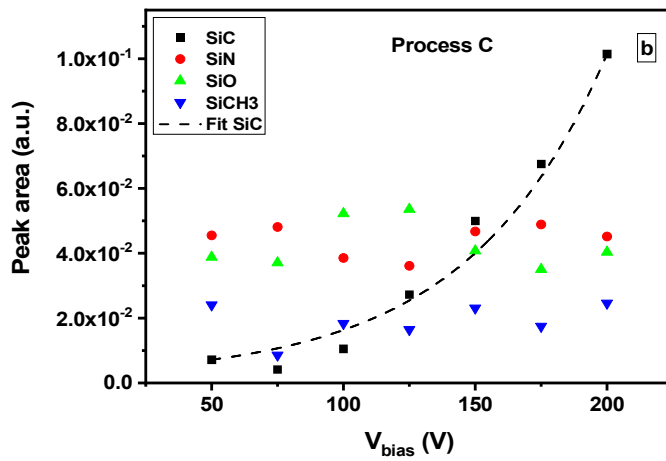
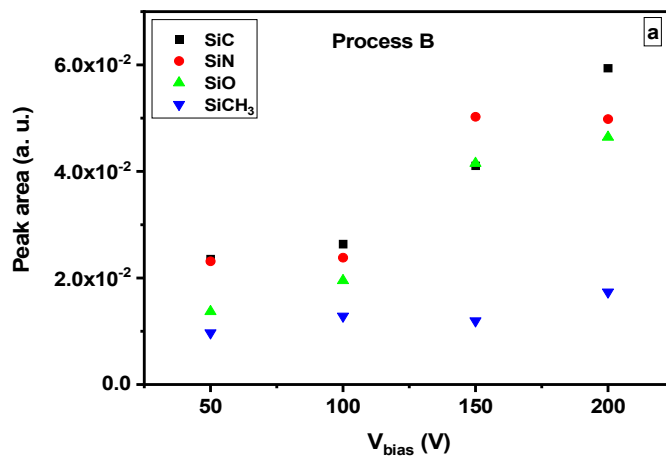
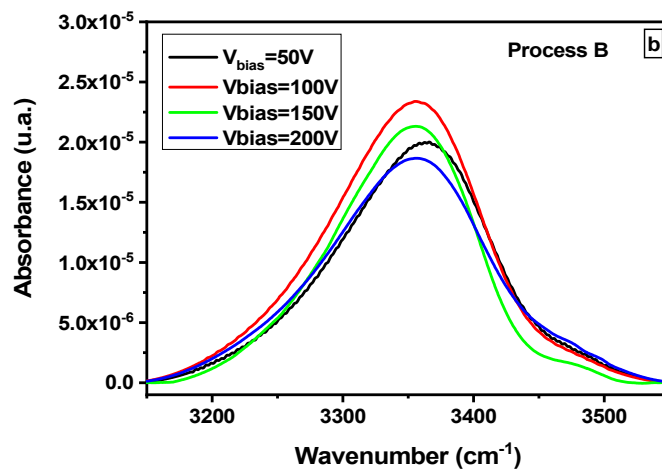
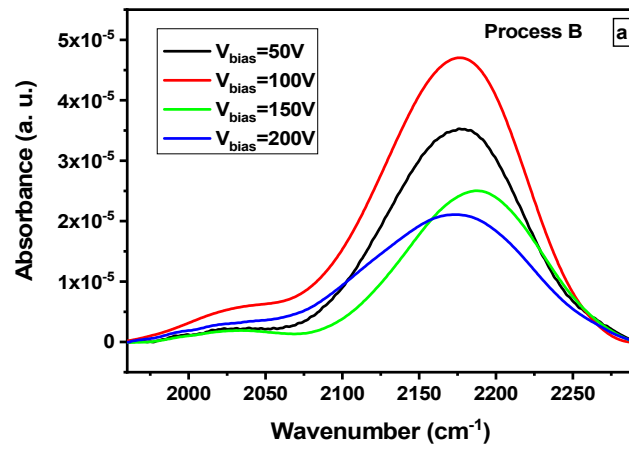


Figure 13



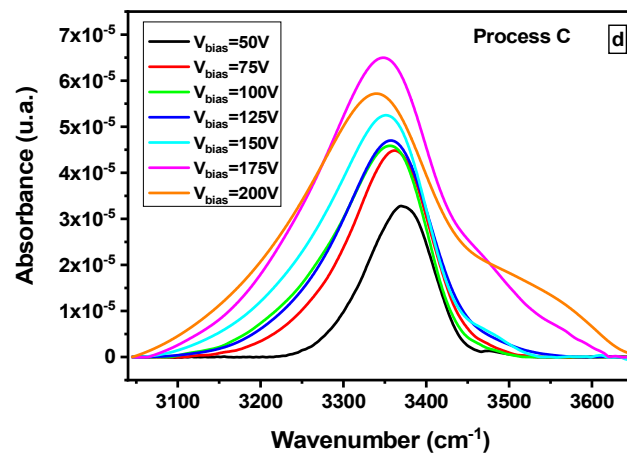
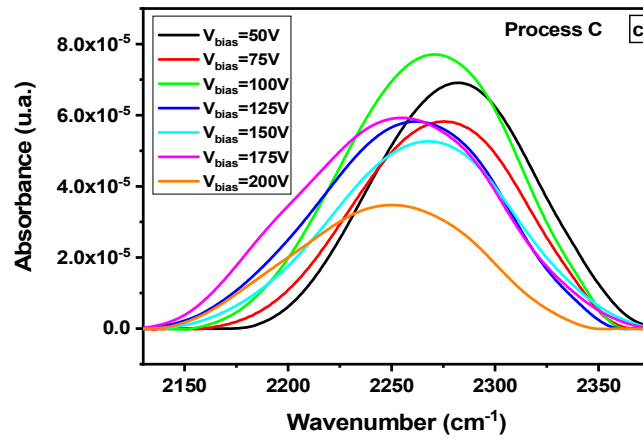


Figure 14

List of table captions

Table 1: OES emitting lines in the visible range from Ar/N₂/Si(CH₃)₄ gas mixture dual plasma.

Table 2: Absorbing FTIR bands considered for FTIR spectra deconvolution of the finger print zone, and SiH and NH bands according to [29 and ref there in].

Table 3: Sample name and autopolarisation voltage V_{bias} corresponding to the process B (RF magnetron plasma) and C (ECR/RF magnetron plasma).

Species and system series	Transition and energy (eV)	Line or Band head wavelength (nm)
Ar	4p → 4s 13.48 → 11.83	750.4
Ar	4s → 4p	696.5
Ar	4s → 5p	811.5
Ar ⁺	² D ₀ → ² P	472.5
Si I	4s ¹ P → 3p ² ¹ D 5.08 → 0.78	288.2 and 5 lines around 250 nm
C ₂ Swan band system	A ₃ Π _g → X' ₃ Π _u	516.5
CN violet system	B ₂ Σ ⁺ (v' = 0) → X ₂ Σ ⁺ (v''=0)	384.0 – 388.4
N ₂ 2 nd positive	C ₃ Π _u (v' = 0) → B ₃ Π _g (v''=0) 11.05 → 7.39	337.1
NH	A ₃ Π (v' = 0) → X ₃ Σ ⁻ (v''=0) 3.7 → 0.0	336.0
H _α Balmer line	3d → 2p 12.09 → 10.20	656.3
H ₂ Fulcher system	d ³ Π _u → a ³ Σ _g	570 - 640

Table 1

Absorbing band	Wavenumber (cm ⁻¹)
SiC (strech.)	800 to 860
SiH (bend.)	900 to 970
SiN (strech.)	970 to 1100
SiO (strech.)	1100 to 1150
NH (bend.)	1150 to 1200
SiCH ₃ (sym. bend.)	1225 to 1280
SiH (stretch.)	2100-2200
NH (stretch.)	3200-3400

Table 2

Process B		Process C			
Sample	V _{Bias} (V)	Sample	V _{Bias} (V)	Sample	V _{Bias} (V)
B50	50	C5	5	C125	125
B100	100	C50	50	C150	150
B150	150	C75	75	C175	175
B200	200	C100	100	C200	200

Table 3

Supplementary data

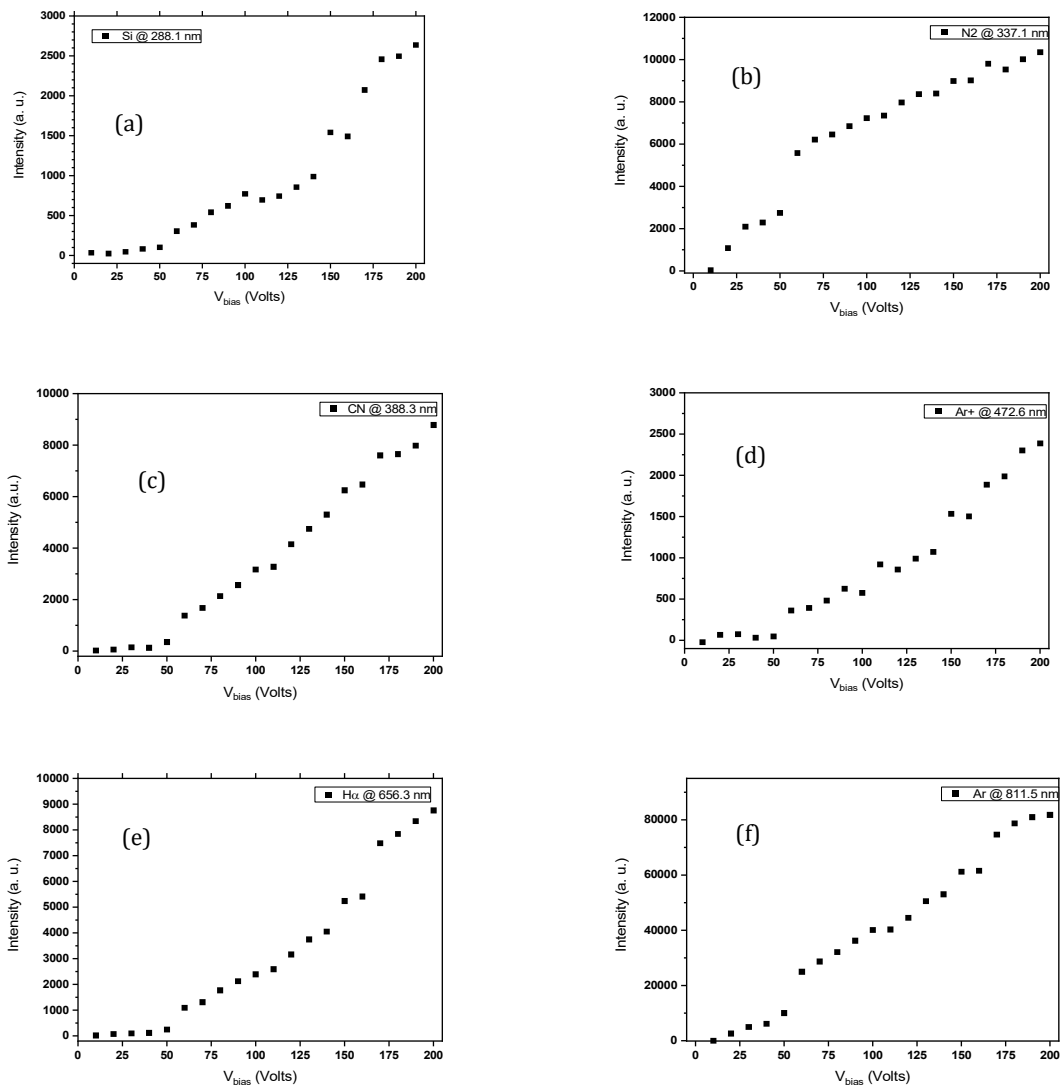


Figure 1 : OES lines analysis for the process B.

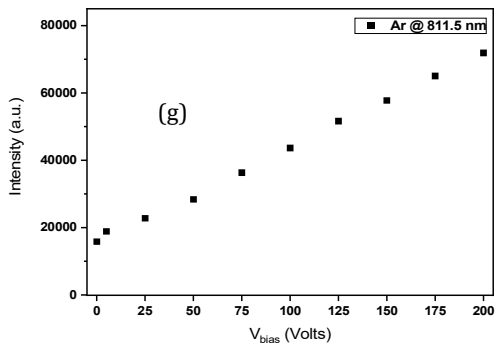
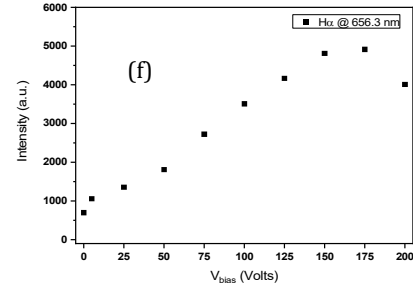
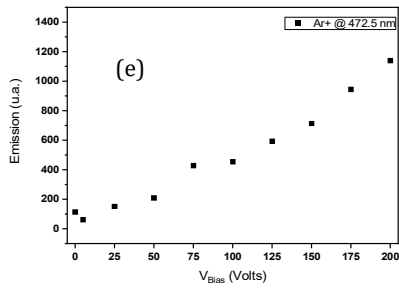
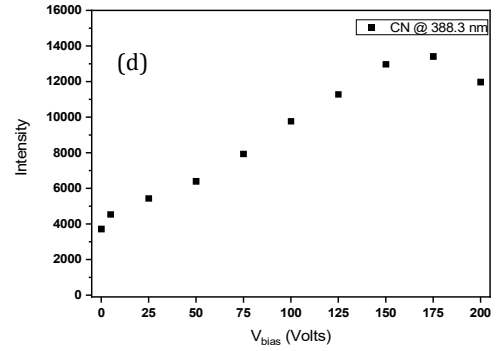
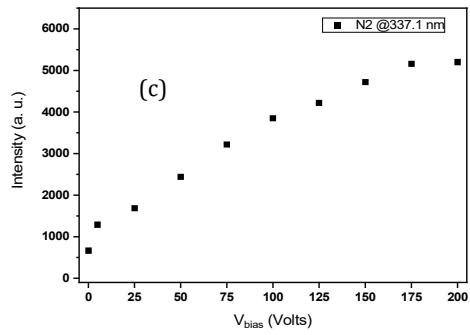
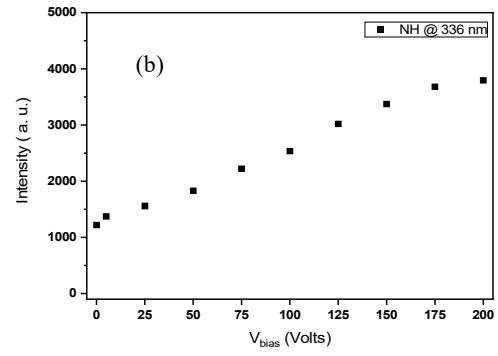
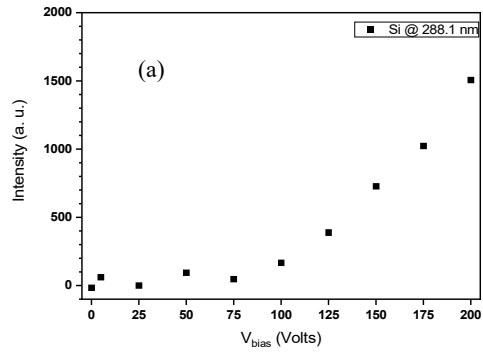


Figure 2 : OES lines analysis for the process C

References

- [1] A. Y. Liu et M. L. Cohen, Prediction of New Low Compressibility Solids, *Science* 245 (1989) 841-842. <https://doi.org/10.1126/science.245.4920.841>.
- [2] A. Badzian et T. Badzian, Recent Developments in Hard Materials, *Int. J. of Refractory Metals & Hard Materials* 15 (1997) 10. [https://doi.org/10.1016/S0263-4368\(96\)00047-9](https://doi.org/10.1016/S0263-4368(96)00047-9).
- [3] A. Badzian, T. Badzian, W. D. Drawl, et R. Roy, Silicon carbonitride: a rival to cubic boron nitride, *Diamond and Related Materials* 7 (1998) 1519-1525. [https://doi.org/10.1016/S0925-9635\(98\)00228-3](https://doi.org/10.1016/S0925-9635(98)00228-3).
- [4] P. Kouakou, M. Belmahi, V. Brien, V. Hody, H.-N. Migeon, et J. Bougdira, Role of silicon on the growth mechanisms of CN_x and SiCN thin films by N_2/CH_4 microwave plasma assisted chemical vapour deposition, *Surface and Coatings Technology*, 203 (2008) 277. <https://doi.org/10.1016/j.surfcoat.2008.09.002>.
- [5] Jan Tomastik, Radim Ctvrtlik, Tomas Ingr, Jan Manak, Ariana Opletalova, Effect of Nitrogen Doping and Temperature on Mechanical, Durability of Silicon Carbide Thin Films, *Scientific Reports* 8(2018) 10428. <https://doi.org/10.1038/s41598-018-28704-3>.
- [6] L. C. Chen, K. H. Chen, S. L. Wei, P. D. Kichambare, J. J. Wu, T. R. Lu, C. T. Kuo, Crystalline SiCN: a hard material rivals to cubic BN, *Thin Solid Films*, 355-356(1999), 112. [https://doi.org/10.1016/S0040-6090\(99\)00490-3](https://doi.org/10.1016/S0040-6090(99)00490-3)
- [7] Alain E. Kaloyeros, Fernando A. Jove, Jonathan Goff, Barry Arkles, Silicon Nitride and Silicon Nitride-Rich Thin Film Technologies: Trends in Deposition Techniques and Related Applications, *ECS Journal of Solid State Science and Technology*, 6 (2017) 691. <https://doi.org/10.1149/2.0011710jss>.
- [8] Aleksander M. Wrobel, Pawel Uznanski, Hard silicon carbonitride thin-film coatings by remote hydrogen plasma chemical vapor deposition using aminosilane and silazane precursors. 2: Physical, optical, and mechanical properties of deposited films, *Plasma Process Polym.* 18(2021) e2000241. <https://doi.org/10.1002/ppap.202000241>.
- [9] B. Plujat, H. Glénat, J. Hamon, Y. Gazal, A. Gouillet, E. Hernandez, S. Quoizola, L. Thomas, Near-field scanning microscopy and physico-chemical analysis versus time of

SiCN:H thin films grown in Ar/NH₃/TMS gas mixture using MW-Plasma CVD at 400 °C, Plasma. Process. Polym. 15 (2018) 1800066. <https://doi.org/10.1002/ppap.201800066>.

[10] P. Kouakou, P. Yoboue, B. Ouattara, V. Hody, P. Choquet, M. Belmahi, Silicon Carbon Nitride Thin Films Produced by Magnetron Reactive Sputtering: Physical Vapour Deposition: Structural, Chemical and Mechanical Characterisation, J. Surface Sci. Technol. 33(2017) 44. <https://doi.org/10.18311/jsst/2017/11022>.

[11] H. Y. Chang, C. Y. Meng, C. W. Huang, S. C. Lee, The low-temperature α -SiN_x films with high impermeability and high optical gap with application to organic light-emitting diode, J. Appl. Phys. 98 (2005) 084501. <https://doi.org/10.1063/1.2089161>.

[12] S. Bulou, L. Le Brizoual, P. Miska, L. de Poucques, J. Bougdira, M. Belmahi, Wide variations of SiC_xN_y:H thin films optical constants deposited by H₂/N₂/Ar/hexamethyldisilazane microwave plasma, Surf. Coat. Technol. 208 (2012) 46. <https://doi.org/10.1016/j.surfcoat.2012.07.079>.

[13] S. Bulou, L. Le Brizoual, P. Miska, L. de Poucques, R. Hugon, M. Belmahi, J. Bougdira, The influence of CH₄ addition on composition, structure and optical characteristics of SiCN thin films deposited in a CH₄/N₂/Ar/hexamethyldisilazane microwave plasma, Thin Solid Films 520 (2011) 245. <https://doi.org/10.1016/j.tsf.2011.07.054>.

[14] Z. Khatami, P. R. J. Wilson, J. Wojcik, et P. Mascher, The influence of carbon on the structure and photoluminescence of amorphous silicon carbonitride thin films, Thin Solid Films 622 (2017) 1. <https://doi.org/10.1016/j.tsf.2016.12.014>.

[15] S. Peter, S. Bernütz, S. Berg, et F. Richter, FTIR analysis of a-SiCN:H films deposited by PECVD, Vacuum 98 (2013) 81. <https://doi.org/10.1016/j.vacuum.2013.04.014>.

[16] Danielle Ngoue, Antoine Grosjean, Laurie Di Giacomo, Sebastien Quoizola, Audrey Soum-Glaude, Laurent Thomas, Yasmine Lalau, Reine Reoyo-Prats, Bernard Claudet, Olivier Faugeroux, Cedric Leray, Adrien Toutant, Jean-Yves Peroy, Alain Ferriere, Gabriel Olalde Ceramics for concentrated solar power (CSP): From thermophysical properties to solar absorbers, Ed. Olivier Guillon In Elsevier Series on Advanced Ceramic Materials, Advanced Ceramics for Energy Conversion and Storage, (2020) 89. <https://doi.org/10.1016/B978-0-08-102726-4.00003-X>.

[17] Aissatou Diop, Danielle Ngoue, Amine Mahammou, Babacar Diallo, Béatrice Plujat, Angélique Bousquet, Thierry Sauvage, Sébastien Quoizola, Mireille Richard-Plouet,

Jonathan Hamon, Audrey Soum-Glaude, Eric Tomasella, Laurent Thomas, Comprehensive study of WSiC:H coatings synthesized by microwave-assisted RF reactive sputtering, *Surface and Coatings Technology* 459 (2023) 129408. <https://doi.org/10.1016/j.surfcoat.2023.129408>

[18] A. Grill, S. M. Gates, T. E. Ryan, S. V. Nguyen, et D. Priyadarshini, Progress in the development and understanding of advanced low k and ultralow k dielectrics for very large-scale integrated interconnects—State of the art, *Applied Physics Reviews* 1 (2014) 011306. <https://doi.org/10.1063/1.4861876>.

[19] Mikhail R. Baklanov, Jean-Francois de Marneffe, Denis Shamiryan, Adam M. Urbanowicz, Hualiang Shi, Tatyana V. Rakhimova, Huai Huang, Paul S. Ho, Plasma processing of low-k dielectrics, *J. Appl. Phys.* 113 (2013) 041101. <https://doi.org/10.1063/1.4765297>.

[20] E. Ermakova, M. Kosinova, Organosilicon compounds as single-source precursors for SiCN films production, *Journal of Organometallic Chemistry* 958 (2022) 122183. <https://doi.org/10.1016/j.jorganchem.2021.122183>.

[21] N. I. Fainer, A. G. Plekhanov, A. N. Golubenko, Yu. M. Rumyantsev, V. I. Rakhlin, E. A. Maximovski, V. R. Shayapov, PECVD Synthesis of Silicon Carbonitride Layers Using Methyltris(diethylamino)silane as the New Single-Source Precursor, *ECS Journal of Solid State Science and Technology* 4 (2015) 3153. <https://doi.org/10.1149/2.0201501jss>.

[22] J. Vlček, M. Kormunda, J. Čížek, V. Peřina, J. Zemek, Influence of nitrogen–argon gas mixtures on reactive magnetron sputtering of hard Si–C–N films, *Surf. Coat. Technol.* 160 (2002) 74. [https://doi.org/10.1016/S0257-8972\(02\)00328-6](https://doi.org/10.1016/S0257-8972(02)00328-6).

[23] J. Vlček, M. Kormunda, J. Čížek, Z. Soukup, V. Peřina, et J. Zemek, Reactive magnetron sputtering of Si–C–N films with controlled mechanical and optical properties, *Diamond and Related Materials* 12 (2003) 1287. [https://doi.org/10.1016/S0925-9635\(03\)00078-5](https://doi.org/10.1016/S0925-9635(03)00078-5).

[24] E. Tomasella, L. Spinelle, A. Bousquet, F. Rebib, M. Dubois, C. Eypert, J. P. Gaston, J. Cellier, et T. Sauvage, Structural and Optical Investigations of Silicon Carbon Nitride Thin Films Deposited by Magnetron Sputtering, *Plasma Processes and Polymers* 6 (2009) S11. <https://doi.org/10.1002/ppap.200930103>.

- [25] X. Xiao, Y. Li, L. Song, X. Peng, et X. Hu, Structural analysis and microstructural observation of SiC_xN_y films prepared by reactive sputtering of SiC in N_2 and Ar, *Applied Surface Science* 156 (2000) 155. [https://doi.org/10.1016/S0169-4332\(99\)00493-6](https://doi.org/10.1016/S0169-4332(99)00493-6).
- [26] X.-W. Du, Y. Fu, J. Sun, P. Yao, et L. Cui, Intensive light emission from SiCN films by reactive RF magnetron sputtering, *Materials Chemistry and Physics* 103 (2007) 456. <https://doi.org/10.1016/j.matchemphys.2007.02.053>.
- [27] Rafaiel A. Ovanesyan, Noemi Leick, Kathryn M. Kelchner, Dennis M. Hausmann, Sumit Agarwal, Atomic Layer Deposition of SiC_xN_y Using Si_2Cl_6 and CH_3NH_2 Plasma, *Chem. Mater.* 29 (2017) 6269. <https://doi.org/10.1021/acs.chemmater.7b01358>.
- [28] Rafaiel A. Ovanesyan, Dennis M. Hausmann, Sumit Agarwal, “A Three-Step Atomic Layer Deposition Process for SiN_x Using Si_2Cl_6 , CH_3NH_2 , and N_2 Plasma”, *ACS Appl. Mater. Interfaces* 10(2018) 19153. <https://doi.org/10.1021/acsami.8b01392>
- [29] M. Belmahi, S. Bulou, A. Thouvenin, L. de Poucques, R. Hugon, L. Le Brizoual, P. Miska, D. Geneve, J. L. Vasseur, J. Bougdira, Microwave Plasma Process for SiCN:H Thin Films Synthesis with composition varying from SiC:H to SiN:H in $\text{H}_2/\text{N}_2/\text{Ar}/\text{Hexamethyldisilazane}$ gas mixture, *Plasma Processes and Polymers* 11(2014) 551. <https://doi.org/10.1002/ppap.201300166>.
- [30] R. Coustel, M. Haacké, V. Rouessac, E. André, S. Roualdès, et A. Julbe, Vibrational frequencies of hydrogenated silicon carbonitride: A DFT study, *Surface and Coatings Technology* 325 (2017) 437. <https://doi.org/10.1016/j.surfcoat.2017.06.017>.
- [31] J. Legrand, P. Pigeat, T. Easwarakhanthan, et H. Rinnert, Structural and optical properties of magnetron-sputtered Er-doped AlN films grown under negative substrate bias, *Applied Surface Science* 307 (2014) 189. <https://doi.org/10.1016/j.apsusc.2014.04.013>.
- [32] R. Swanepoel, Determination of surface roughness and optical constants of inhomogeneous amorphous silicon films, *Journal of Physics E: Scientific Instruments*, 17 (1984) 896. <https://doi.org/10.1088/0022-3735/17/10/023>.
- [33] A. Thouvenin, Dépôt et caractérisation de couches minces de $\text{SiC}_x\text{N}_y\text{H}$ par CVD assistée par plasma micro-ondes ECR avec précurseurs organosiliciés, Phd Thesis (2016), Université de Lorraine, France (in French).

- [34] Z. Al Hallak, Synthèse et caractérisation de films minces de $\text{SiC}_x\text{N}_y\text{H}$ par procédé CVD assisté par plasma ECR/Magnétron RF, Phd Thesis (2021), Université de Lorraine, France (in French).
- [35] Maksim N. Chagin, Veronica S. Sulyaeva, Vladimir R. Shayapov, Aleksey N. Kolodin, Maksim N. Khomyakov, Irina V. Yushina, Marina L. Kosinova, Synthesis, Properties and Aging of ICP-CVD $\text{SiC}_x\text{N}_y\text{H}$ Films Formed from Tetramethyldisilazane, *Coatings* 12 (2022) 80. <https://doi.org/10.3390/coatings12010080>.
- [36] Hieronim Szymanowski, Katarzyna Olesko, Jacek Kowalski, Mateusz Fijalkowski, Maciej Gazicki-Lipman, Anna Sobczyk-Guzenda, “Thin SiNC/SiOC coatings with a gradient of refractive index deposited from organosilicon precursor”, *Coatings* 10 (2020) 794. <https://doi.org/10.3390/coatings10080794>.
- [37] M. Milosevic, S. L. Berets, Applications of the theory of Optical Spectroscopy to numerical simulations, *Applied Spectroscopy* 47 (1993) 566. <https://doi.org/10.1366/0003702934067117>.
- [38] Milan Milosevic, Sean W. King, Validation of a correction procedure for removing the optical effects from transmission spectra of thin films on substrates, *Journal of Applied Physics* 112 (2012) 093514. <https://doi.org/10.1063/1.4764346>.
- [39] G. Lavaredaa, Y. Vygranenko, A. Amaral, C. Nunes de Carvalho, N. P. Barradase, E. Alves, P. Brogueira, Dependence of optical properties on composition of silicon carbonitride thin films deposited at low temperature by PECVD, *Journal of Non-Crystalline Solids* 551 (2021) 120434. <https://doi.org/10.1016/j.jnoncrysol.2020.120434>.
- [40] Ludovic de Poucques, Jean-Christophe Imbert, Caroline Boisse-Laporte, Petr Vasina, Jean Bretagne, Lionel Teulé-Gay, Michel Touzeau, Spatial characterization of an IPVD reactor: neutral gas temperature and interpretation of optical spectroscopy measurements, *Plasma Sources Sci. Technol.* 14 (2005) 321. <https://doi.org/10.1088/0963-0252/14/2/014>.
- [41] S. Peter, F. Speck, M. Lindner, T. Seyller, Analysis of a-SiCN:H films by X-ray photoelectron spectroscopy, *Vacuum* 138 (2017) 191. <https://doi.org/10.1016/j.vacuum.2016.09.016>.
- [42] S.-H. Bang, Jae-Ho Suk, Kun-Su Kim, Jong-Hwan Park, Nong-Moon Hwang, Effects of radio frequency power and gas ratio on barrier properties of SiO_xN_y films deposited by

inductively coupled plasma chemical vapor deposition, *Thin Solid Films* 669 (2019) 108.
<https://doi.org/10.1016/j.tsf.2018.10.016>.

[43] S. Peter, R. Ehrler, T. Seyller, F. Speck, Annealing effects on a-SiC:H and a-SiCN:H films deposited by plasma CVD methods, *Vacuum* 178 (2020) 109410.
<https://doi.org/10.1016/j.vacuum.2020.109410>.

[44] A. Bachar, A. Bousquet, H. Mehdi, G. Monier, C. Robert-Goumet, L. Thomas, M. Belmahi, A. Goulet, T. Sauvage, E. Tomasella, Composition and optical properties tunability of hydrogenated silicon carbonitride thin films deposited by reactive magnetron sputtering, *Applied Surface Science* 444 (2018) 293.
<https://doi.org/10.1016/j.apsusc.2018.03.040>.

[45] Jingxin Jian, Jianwu Sun, A Review of Recent Progress on Silicon Carbide for Photoelectrochemical Water Splitting, *Sol. RRL* 4 (2020) 2000111.
<https://doi.org/10.1002/solr.202000111>.